Motion of a rod-like particle between parallel walls with application to suspension rheology

Article *in* Journal of Rheology · January 2007

DOI: 10.1122/1.2399084

CITATIONS
28

READS
122

3 authors:

Mauricio Zurita-Gotor
Abengoa
26 PUBLICATIONS **685** CITATIONS
SEE PROFILE

Jerzy Blawzdziewicz
Texas Tech University
138 PUBLICATIONS **2,135** CITATIONS
SEE PROFILE

Eligiusz Wajnryb
Polish Academy of Sciences
131 PUBLICATIONS **2,886** CITATIONS
SEE PROFILE

Motion of a rod-like particle between parallel walls with application to suspension rheology

M. Zurita-Gotor[a)] and J. Bławzdziewicz

Department of Mechanical Engineering, Yale University, P.O. Box 20-8286, New Haven, Connecticut 06520

E. Wajnryb

Institute of Fundamental Technological Research, Polish Academy of Sciences, Świętokrzyska 21, 00-049 Warszawa, Poland

(Received 17 March 2006; final revision received 17 October 2006)

Synopsis

We study the dynamics of elongated axisymmetric particles undergoing shear flow between two parallel planar walls, under creeping-flow conditions. Particles are modeled as linear chains of touching spheres and it is assumed that walls are separated by a distance comparable to particle length. The hydrodynamic interactions of the chains with the walls are evaluated using our Cartesian-representation algorithm [Bhattacharya *et al.*, Physica A **356**, 294–340 (2005b)]. We find that when particles are far from both walls in a weakly confined system, their trajectories are qualitatively similar to Jeffery orbits in unbounded space. In particular, the periods of the orbits and the evolution of the azimuthal angle in the flow-gradient plane are nearly independent of the initial orientation of the particle. For stronger confinements, however, (i.e., when the particle is close to one or both walls) a significant dependence of the angular evolution on the initial particle configuration is observed. The phases of particle trajectories in a confined dilute suspension subject to a sudden onset of shear flow are thus slowly randomized due to unequal trajectory periods, even in the absence of interparticle hydrodynamic interactions. Therefore, stress oscillations associated with initially coherent particle motions decay with time. The effect of near contact particle-wall interactions on the suspension behavior is also discussed. © *2007 The Society of Rheology.*
[DOI: 10.1122/1.2399084]

I. INTRODUCTION

The effect of confining walls on the hydrodynamic behavior of particles suspended in a viscous fluid is relevant for a wide range of problems: for instance, blood microcirculation [Das *et al.* (1997); Goldsmith and Spain (1984); Perktold (1987); Pries *et al.* (1989)], propagation of colloids in the natural environment [Loveland *et al.* (2003)], development of new methods for particle separations [Giddings (1993); Huang *et al.* (2004); Regazzetti *et al.* (2004)], and manipulation of particles in microfluidic devices [Whitesides and Stroock (2001)]. Hydrodynamic confinement effects in particulate systems are studied to explain the collective motion of suspended particles [Cohen *et al.*

[a)]Author to whom correspondence should be addressed; electronic mail: mauricio.zurita-gotor@aya.yale.edu

(2004); Hernández-Ortiz *et al.* (2005); Lin *et al.* (2000); Mucha *et al.* (2004); Nguyen and Ladd (2005)], as well as to characterize the wall effects on the motion of single particles which are spherical [Dufresne *et al.* (2001); Lançon *et al.* (2001)] or nonspherical [Gavze and Shapiro (1997, 1998); Hsu and Ganatos (1994); Mody and King (2005); Pozrikidis (2005); Staben *et al.* (2006)]. Such problems have also been analyzed in a series of our recent publications [Bhattacharya *et al.* (2005a,2005b; 2006); Bławzdziewicz and Bhattacharya (2003)].

Our present study is focused on the effect of confinement on the motion of individual particles and the corresponding rheological response in a dilute suspension of elongated, axisymmetric, non-Brownian particles in creeping flow between two parallel walls. The suspension is subject to a constant shear flow that results from the relative motion of the walls. These conditions occur in various engineering systems and the problem can be experimentally studied in a constant-shear-flow rheometer [Bird *et al.* (1977)].

The size of the particles (modeled here as rigid linear arrays of spheres) is assumed to be comparable to the wall separation. We consider the low-concentration regime where the particles are hydrodynamically coupled to the walls but not to each other. Thus, interparticle interactions are entirely neglected (the effect of binary particle collisions on the suspension evolution will be described elsewhere).

The dynamics of elongated particles undergoing shear flow in unbounded space was first described by Jeffery (1922) in his early work on ellipsoids. Jeffery's result was later generalized for arbitrary axisymmetric particles by Bretherton (1962). Their research has demonstrated that isolated axisymmetric particles in shear flow undergo a periodic tumbling motion with a period that is independent of the initial orientation of the particle.

Hence, in a dilute suspension under shear, not only do individual noninteracting particles exhibit periodic motions, but also the entire particle distribution evolves periodically. The associated ensemble-averaged quantities (such as the particle contribution to the effective stress) are periodic as well. In particular, an initially isotropic particle distribution is time dependent, because elongated particles in shear flow spend most of the time near the flow-vorticity plane (according to Jeffery's result).

At small but finite concentrations, the oscillations of the particle distribution slowly decrease because hydrodynamic interactions between particles perturb individual particle trajectories. The cumulative effect of such perturbations can be described using, e.g., a Fokker–Planck approach [Brenner (1974), Kim and Karrila (1991); Petrie (1999)]. The oscillations also decay in the presence of angular Brownian motion.

In contrast, in a wall-bounded system the oscillations of the particle distribution decay even for non-Brownian particles at infinitesimal suspension concentrations, because periods of particle trajectories depend on the particle orientation and position with respect to the walls. A quantitative analysis of wall effects on individual particle trajectories and the resulting time-dependent rheological response is the focus of our study.

Our model system, its hydrodynamic description, and our simulation method are described in Sec. II. In Sec. III we characterize the effect of confinement on the particle velocities and effective stress in a dilute suspension of spheres. Section IV presents our analysis of the behavior of individual chains of spheres in a confined shear flow. The consequences of this behavior for suspension rheology are discussed in Sec. V, where response of the system to a sudden onset of shear flow is investigated. The concluding remarks are given in Sec. VI.

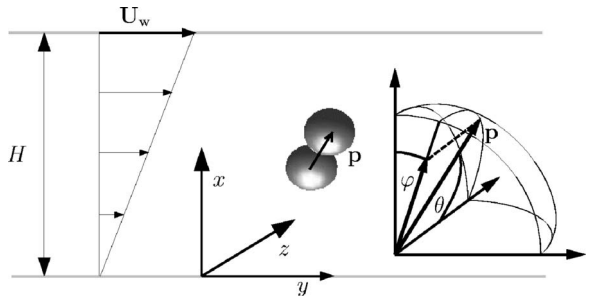

FIG. 1. Coordinate systems used to describe the position (x,y,z) and orientation $\mathbf{p}$ of a linear chain of equal-size touching spheres of diameter d. The chain orientation is characterized by the spherical coordinates (θ,φ), where θ is the angle between $\mathbf{p}$ and the vorticity axis z, and φ is the angle between the projection of $\mathbf{p}$ onto the velocity-gradient plane y-x and the gradient direction x.

II. MODEL SYSTEM: CONFINED SUSPENSION OF NON-INTERACTING LINEAR CHAINS OF SPHERES

A. Hydrodynamic description

We consider motion of elongated, axisymmetric rigid particles undergoing stationary shear flow in a space bounded by two parallel planar walls. We focus on configurations where the wall separation H is comparable to particle length. The suspending fluid has viscosity η and creeping-flow conditions are assumed. Our one-particle results are applied to determine the effect of confinement on rheological response of a dilute suspension of elongated, rod-like particles.

We use here a coordinate system where the walls are parallel to the y-z plane. The unperturbed fluid velocity

$$\mathbf{v}^{\text{ext}}(\mathbf{r}) = \dot{\gamma} x \hat{\mathbf{e}}_y \tag{1}$$

(where $\dot{\gamma}$ denotes the shear rate) points in the lateral direction y, and varies in the normal direction x. The flow occurs due to the motion of one of the walls with the velocity

$$\mathbf{U}_w = \dot{\gamma} H \hat{\mathbf{e}}_y \tag{2}$$

(as in a parallel-wall rheometer). Particles are torque and force free. No-slip boundary conditions are imposed at both walls and at the particle surfaces. The geometry of the system is depicted in Fig. 1.

The present study focuses on the behavior of axisymmetric particles modeled as linear chains of N equal-size touching spheres of diameter d. We note that particle doublets [Johnson *et al.* (2005)] and multiparticle conglomerates of spheres (including long linear chains) can be synthesized in a controlled way, for example using a template-assisted self-assembly process [Xia *et al.* (2003)]. Our quantitative results thus directly apply to such particles, whereas our general qualitative conclusions are also valid for rod-like particles of other shapes.

Given the linearity of Stokes equations, the translational and angular particle velocities $\mathbf{U}_i$ and $\mathbf{\Omega}_i$, as well as the stresslet $\mathbf{S}_i$ induced on the surface of particle i, are linearly related to the external flow (1). This linear relation can be represented in the form

$$\begin{pmatrix} \mathbf{U}_i \\ \boldsymbol{\Omega}_i \\ \mathbf{S}_i \end{pmatrix} = \begin{pmatrix} \boldsymbol{\nu}_i^{\mathrm{ts}} \\ \boldsymbol{\nu}_i^{\mathrm{rs}} \\ \boldsymbol{\nu}_i^{\mathrm{ss}} \end{pmatrix} \dot{\gamma}, \tag{3}$$

where $\boldsymbol{\nu}_i^{\mathrm{ts}}$, $\boldsymbol{\nu}_i^{\mathrm{rs}}$, and $\boldsymbol{\nu}_i^{\mathrm{ss}}$ denote appropriate hydrodynamic mobility functions. Our present study is focused on suspensions in infinite-dilution limit, and therefore we assume that there are no hydrodynamic interactions between individual particles. Accordingly, the mobility coefficients

$$\boldsymbol{\nu}_i^{\alpha s} = \boldsymbol{\nu}^{\alpha s}(\mathbf{r}_i, \mathbf{p}_i), \quad \alpha = t, r, s, \tag{4}$$

depend only on the orientation $\mathbf{p}_i$ and position $\mathbf{r}_i$ of the center of symmetry of particle i, but not on the configuration of other particles in the system. Note, however, that the hydrodynamic interactions between the spheres within each chain are included in our analysis.

Hydrodynamic mobility functions (4) are calculated using our recently developed Cartesian-representation method [Bhattacharya *et al.* (2005a, 2005b, 2006)] for evaluating hydrodynamic interactions between many spheres in the parallel-wall geometry. Our method relies on expanding the flow field in the system both in Cartesian and spherical basis of Stokes flow. The Cartesian basis is used to evaluate the flow field scattered from the walls and the spherical basis to describe the interaction of the fluid with the spheres. The two basis sets of flow fields are related to each other by an appropriate set of transformations. In practical calculations, the spherical basis is truncated at a relatively low spherical-harmonics order L. To assure good convergence of the method for small particle-wall gaps, the particle-wall lubrication corrections are included in a pair superposition approximation [Cichocki *et al.* (2000); Durlofsky *et al.* (1987)]. We note that for rigid arrays of spheres, the sphere-sphere lubrication corrections are not needed.

Appropriate hydrodynamic functions evaluated using Cartesian-representation technique are combined into the chain mobility coefficients (4) by requiring that the whole chain move as a rigid body and that the net force and torque acting on the chain vanish. The stresslet $\mathbf{S}_i$ of the whole chain is calculated as the sum of the hydrodynamic stresslets $\mathbf{S}^{(k)}$ centered on individual spheres and the stresslets associated with hydrodynamic forces resulting from the rigid-body constraints

$$\mathbf{S}_i = \sum_{k=1}^{N} \mathbf{S}^{(k)} + \sum_{k=1}^{N} \left[\mathbf{F}^{(k)} \mathbf{r}^{(k)}\right]_d. \tag{5}$$

Here $\mathbf{F}^{(k)}$ denotes the force acting on a sphere k, $\mathbf{r}^{(k)}$ is the position of the center of this sphere, and $[\ldots]_d$ denotes the deviatoric part of a tensor. Note that for force-free chains, relation (5) is independent of the choice of the reference point with respect to which the positions of the spheres are evaluated.

In our simulations, the translational and angular velocities $\mathbf{U}_i$ and $\boldsymbol{\Omega}_i$ are numerically integrated to determine particle trajectories by the procedure outlined in Sec. II B. The stresslets $\mathbf{S}_i$ are then used to evaluate the rheological response of a dilute suspension of particles [Kim and Karrila (1991)]

$$\boldsymbol{\sigma}^{\mathrm{eff}} = -p^{\mathrm{eff}}\mathbf{I} + 2\eta\mathbf{E} + \boldsymbol{\sigma}', \tag{6}$$

where $\boldsymbol{\sigma}^{\mathrm{eff}}$ is the effective stress in the suspension, p^{eff} denotes the effective pressure, $\mathbf{I}$ is the identity tensor, and $\mathbf{E} = \frac{1}{2}\dot{\gamma}(\hat{\mathbf{e}}_x\hat{\mathbf{e}}_y + \hat{\mathbf{e}}_y\hat{\mathbf{e}}_x)$ is the strain-rate tensor associated with the flow (1). In the above relation, the quantity

$$\boldsymbol{\sigma}' = n_p\langle \mathbf{S} \rangle = \frac{1}{V}\sum_{i=1}^{N_p} \mathbf{S}_i \tag{7}$$

represents the particle contribution to the deviatoric stress, where V is the volume of the system, N_p denotes the number of particles, $n_p = N_p/V$ is the particle number density, and the bracket denotes the ensemble average. In general, the sum on the right side of Eq. (7) involves averaging over statistical realizations of the system, in addition to summation over the particles but for infinitely diluted suspensions, considered herein, this distinction is irrelevant, and the average (7) is computed from N_p independent realizations of single-particle trajectories (cf. discussion in Sec. II C).

We note that Eq. (7) yields the value of the effective stress averaged over the volume of the system. Using the continuity of the momentum flux and the lateral translational symmetry, it can be shown that the shear component σ_{xy} and the normal component σ_{xx} of the stress tensor are position independent. However, in general, the local values of the lateral components σ_{yy} and σ_{zz} may depend on the vertical coordinate x. Typical rheological measurements of the normal-stress differences [e.g., using the method proposed by Kotaka, Kurata, and Tamura (1959)] yield the values averaged across the gap, because the lateral components of the stress are evaluated using momentum continuity equations in a quasi-two-dimensional approximation. Thus, the average quantity defined by Eqs. (6) and (7) corresponds to the stress measured in rheological experiments.

B. Integration of the equation of motion

Particle trajectories are described by the equations of motion

$$\dot{\mathbf{r}} = \mathbf{U}, \tag{8a}$$

$$\dot{\mathbf{p}} = \boldsymbol{\Omega} \times \mathbf{p}, \tag{8b}$$

for the particle position, $\mathbf{r}$ and orientation, $\mathbf{p}$. The equations are numerically integrated after evaluating at each time step the translational and angular velocities $\mathbf{U}$ and $\boldsymbol{\Omega}$ via Eq. (3), as outlined above. (The dot denotes here the derivative with respect to time, and the index i has been dropped for simplicity.)

The evolution equation for particle orientation (8b) is integrated in the spherical coordinate system (θ, φ) where θ is the angle between the particle orientation vector $\mathbf{p}$ and the vorticity axis z, and φ is the angle between the projection of $\mathbf{p}$ onto the velocity-gradient plane y-x and the gradient direction x. This coordinate system (see also the definition Fig. 1) is convenient for the description of particle angular trajectories because in free space the evolution of the azimuthal angle φ is independent of the polar angle θ [Kim and Karrila (1991)]. In wall-bounded systems, the evolution of the azimuthal angle φ is thus expected to be relatively insensitive to the orientation of the particle with respect to the vorticity axis. As shown in Sec. IV A this is indeed the case, provided that the separation between the walls, H, is greater than particle length Nd.

Equation (8b) rewritten in the spherical coordinate system yields

$$\begin{aligned} \dot{\varphi} &= \Omega_z - \cot\theta(\Omega_x \cos\varphi + \Omega_y \sin\varphi), \\ \dot{\theta} &= \Omega_y \cos\varphi - \Omega_x \sin\varphi. \end{aligned} \tag{9}$$

The evolution equations (8a) and (9) have been integrated numerically using the fourth order Runge-Kutta method with adaptive step size [Press *et al.* (1992)]. We note that for large wall separations, the magnitude of the component y of the translational particle

velocity is much larger than other velocity components because the particle is convected with the flow in the y direction. To avoid difficulties in the adaptive time stepping that are associated with large differences in velocity magnitudes, the convective velocity $\mathbf{v}^{\mathrm{ext}}(\mathbf{r})$ is subtracted from the particle velocity $\mathbf{U}$ before each integration step, and the corresponding displacement is added back after the size of the next time step has been computed. Also, the angular equations of motion (9) become singular for $\theta=0$ so an alternative reference frame where the angle θ is measured from the gradient direction is used for the numerical evaluation of trajectories of particles that are nearly aligned with the vorticity direction.

C. Evolution of the statistical ensemble

To determine the rheological response of the suspension, the evolution of an appropriately defined statistical ensemble representing the system has to be evaluated. For dilute suspensions, considered herein, it suffices to represent the system in terms of a set of independent one-particle trajectories with an assumed probability distribution of the initial conditions.

In this paper we focus on the following startup problem: a suspension, initially in thermodynamic equilibrium at rest, is subject to a sudden onset of shear flow. The initial equilibrium distribution can be attained, for example, as a result of weak Brownian motion acting in a quiescent suspension for a sufficiently long time. We assume, however, that after the flow has started, its magnitude is sufficiently large for the Brownian motion to be neglected during the subsequent evolution process. Thus, equations of motion (8) do not have any Brownian corrections.

We note that in the regime of weak Brownian motion the suspension is not always given enough time to equilibrate. The equilibrium distribution can also be distorted due to gravity or other long-range forces. However, if the deviation from equilibrium is not too large, the results presented in Sec. V for suspension rheology should still give a qualitative picture of the system behavior.

A set of independent initial single-particle configurations satisfying the one-particle equilibrium probability distribution $\rho^{\mathrm{eq}}=\rho^{\mathrm{eq}}(x,\theta,\varphi)$ is constructed using a standard Monte Carlo technique [Frenkel and Smit (2002)]. Accordingly, the positions of particle centers are chosen randomly in the space between the walls, and the particle orientations are sampled from the uniform solid angle distribution. Configurations for which the particle overlaps with a wall are rejected. We note that due to this excluded volume the number density of particle centers is smaller near the walls than at the center of the channel, and the particles are predominantly oriented parallel to the walls in the near-wall regions.

In order to evaluate the long-time response of the system, the evolution of the particle ensemble has to be followed for long times. To accelerate the calculations, we utilize the periodicity of particle trajectories (cf. the discussion in Sec. IV A). Accordingly, for each initial condition, the trajectory is numerically integrated only over a single period. The particle configuration and the stresslet calculated at discrete times are then interpolated using cubic splines. Once the trajectory period has been accurately determined, the cubic-spline interpolation function is used to extrapolate stresslets to arbitrarily long times (as required for reaching steady-state conditions for ensemble-averaged quantities).

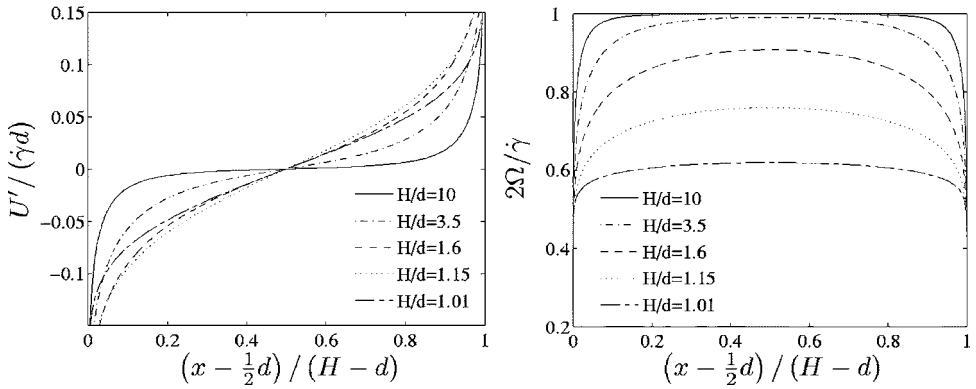

FIG. 2. Normalized linear (left panel) and angular (right panel) velocities of a spherical particle in shear flow between two planar walls, versus particle-wall gap $x-d/2$ scaled by the available space H-d, for different wall separations H. The linear velocity $U'=U-\dot{\gamma}x$ corresponds to particle motion relative to the fluid at particle position.

III. EFFECTS OF CONFINEMENT IN A SUSPENSION OF NONINTERACTING SPHERES

A. Particle velocities

As in the unbounded space, a single sphere in shear flow between two planar walls does not change its vertical position, owing to the symmetry of the system. The particle thus moves with constant linear and angular velocities $\mathbf{U}=U\hat{\mathbf{e}}_y$ and $\mathbf{\Omega}=\Omega\hat{\mathbf{e}}_z$. The dependence of these velocities on the particle position for several values of wall separations H is shown in Fig. 2. The results are plotted versus the particle-wall gap $x-d/2$ scaled by the available space $H-d$.

The results indicate that for weak confinements (e.g., $H/d=10$), particle motion in the middle part of the channel is nearly unaffected by the walls. As expected, particles in this region are convected with the local fluid velocity (1), and rotate with angular velocity $\Omega=\dot{\gamma}/2$. Wall effects are strong when particle-wall separation is of the order of particle size d. In the near-wall regions the particle velocity approaches the wall velocity and particle rotation decreases. However, a complete arrest of the relative particle-wall motion occurs only in very thin logarithmic lubrication layers for the tangential translation and for rotation about an axis parallel to the wall [Kim and Karrila (1991)].

In strongly confined configurations ($H/d\lesssim 3$) wall effects on particle translation and rotation are significant for all vertical particle positions. The angular velocity Ω decays with decreasing wall separation H, and the translational velocity U is strongly affected by the walls everywhere except for the center position $x=H/2$. For $H/d\to 1$, the angular velocity in the center of the channel tends to the limiting value $\Omega=\dot{\gamma}/4$, which follows from the ratio between the magnitudes of the translational and rotational lubrication resistance coefficients in the logarithmic lubrication regime [Cichocki and Jones (1998)].

B. Stress response

Due to the flow-reversal symmetry of Stokes equations and the reflection symmetries of the problem, the only nonzero component of the stresslet induced on the surface of a spherical particle is the shear component S_{xy}. In what follows, this component will be denoted by S^H_{sphere}. Our numerical results for S^H_{sphere}, normalized by its value in an unbounded domain

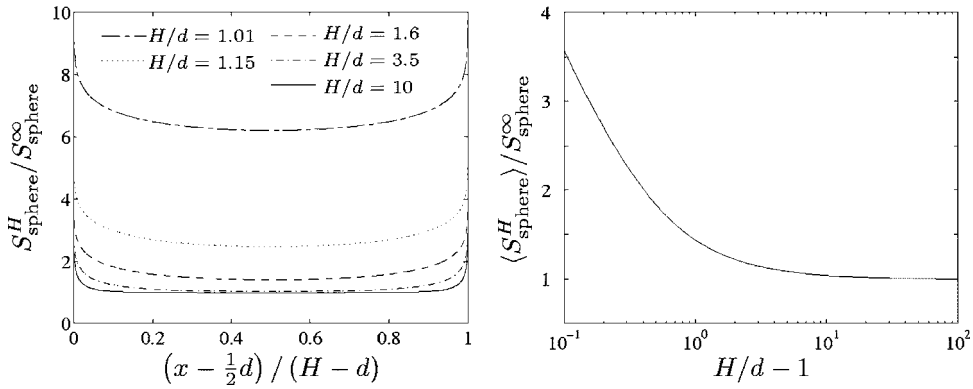

FIG. 3. Particle contribution to the shear stress in a dilute suspension of noninteracting spheres undergoing shear flow between two planar walls. Left panel shows the stresslet S^H_{sphere} induced on an individual sphere, versus scaled particle-wall gap, for different wall separations H. Right panel shows the average stress contribution $\langle S^H_{\text{sphere}}\rangle$ for uniform sphere distribution, versus scaled wall separation $H/d-1$. The results are normalized by the free space value (10).

$$S^\infty_{\text{sphere}} = \tfrac{5}{12}\pi\dot{\gamma}\eta d^3, \tag{10}$$

are plotted in Fig. 3 and listed in Table I. Note that expression (10) is equivalent to the well known Einstein (1906, 1911) result

$$\sigma'^\infty_{xy} = \dot{\gamma}\eta\tfrac{5}{2}\phi, \tag{11}$$

where σ'^∞_{xy} is the particle contribution to the effective stress (6) in free space, and $\phi = \frac{1}{6}\pi n_p d^3$ is the particle volume fraction.

In the left panel of Fig. 3, the stresslet component S^H_{sphere} is plotted versus particle vertical position x for the same values of the nondimensional wall separation H/d as those in Fig. 2. In the right panel, we show the average value $\langle S^H_{\text{sphere}}\rangle$ as a function of H/d (where the average is evaluated with respect to the uniform distribution of spheres in the space between the walls). We recall that the quantity $\langle S^H_{\text{sphere}}\rangle$ is equivalent to the particle contribution to the effective stress, according to Eq. (7).

TABLE I. Normalized particle contribution to the shear stress $\langle S^H_{\text{sphere}}\rangle/S_{\text{sphere}}$ in a dilute uniform suspension of noninteracting spheres undergoing shear flow between two planar walls, for different values of scaled channel width H/d. Convergence of the numerical results with the multipolar truncation order L is also shown.

	Multipolar truncation order L						
H/d	2	3	4	5	6	8	10
1.01	7.224	6.556	6.996	6.602	6.887	6.828	6.785
1.05	4.595	4.060	4.362	4.115	4.265	4.221	4.200
1.2	2.717	2.456	2.543	2.492	2.510	2.505	2.504
1.6	1.718	1.657	1.661	1.658	1.659		
2.4	1.322	1.308	1.306				
3.5	1.182	1.175	1.174				
7	1.076	1.074	1.073				
10	1.051	1.049					

As expected, the stresslet S^H_{sphere} in weakly confined systems deviates from the free-space value only in the near-wall regions (this behavior is similar to the one observed in Fig. 2 for the particle velocities). For $H/d \lesssim 1.5$, the deviation of S^H_{sphere} from S^∞_{sphere} is significant for all particle positions, and S^H_{sphere} diverges logarithmically with $H/d-1$ in the limit $H \to d$. This logarithmic divergence, which follows from the stresses that arise in two lubrication layers between the sphere and the walls [Cichocki and Jones (1998)], is also seen in the right panel for the average stress $\langle S^H_{\text{sphere}} \rangle$.

Accuracy tests of our method for calculating hydrodynamic mobility and resistance functions for systems of spherical particles in wall-bounded creeping flows were presented in our previous publications [Bhattacharya *et al.* (2005a, 2005b, 2006)]. Here we give some additional tests that are relevant for our present study. We recall that the key parameter that controls the accuracy is the maximal order L of the Stokes-flow multipoles included in the calculation. We also recall that the algorithm includes additive particle-wall lubrication corrections.

Table I shows the convergence of the average shear-stress contribution $\langle S^H_{\text{sphere}} \rangle$ with the truncation order L. The results indicate that the convergence is rapid for large wall separations, but it is much slower in the region of small values of H/d. The rapid convergence of $\langle S^H_{\text{sphere}} \rangle$ for $H/d \gtrsim 2$ results not only from a smaller fraction of particles in near-contact configurations but also from a good convergence of the individual stresslet values even if the sphere is very close to a wall. For example, detailed tests indicate that for $H/d=10$, truncation at $L=2$ yields the relative error below 1% for all particle positions in the channel. Therefore, the slower convergence for highly confined systems is due to the interaction between two strongly excited lubrication regions.

In our simulations of linear chains of spheres, discussed below, we only consider configurations with $H/d \gtrsim 2$. We thus use the multipolar truncation level $L=2$, which yields sufficiently accurate results, with the numerical error typically below 5%.

IV. MOTION OF LINEAR CHAINS

Before we go on to describe, in Sec. V, the effect of confinement on the rheology of a suspension of nonspherical particles, we first discuss some important features of individual particle trajectories. This will help us to gain a better insight into the system behavior and determine the conditions under which the rheological response of the suspension does not depend on short-range nonhydrodynamic interactions between the particles and the walls. In Sec. IV A, we first focus on the evolution of particle orientation and the periodicity of particle motion. The evolution of the minimum distance of the particle to one of the walls and the role of near-contact particle-wall interactions are discussed in Secs. IV B and IV C.

A. Angular evolution

Figure 4 depicts the time dependence of the particle orientation vector $\mathbf{p}$ for a short chain with $N=2$ spheres. The orientation is described by the polar and azimuthal angles θ and φ in the spherical coordinate system defined in Sec. II B. We recall that θ is measured with respect to the axis z oriented in the vorticity direction, and φ is the angle in the x-y plane, measured anticlockwise from the gradient direction x. Accordingly, $\varphi = \pi/2$ corresponds to the particle in a plane parallel to the walls (flow-vorticity plane), and $\theta=0$ to the particle oriented along the vorticity direction. The particles are initially in the plane $\varphi=\pi/2$. The results are shown for a set of different initial orientations $\theta_\parallel$ with respect to the vorticity axis.

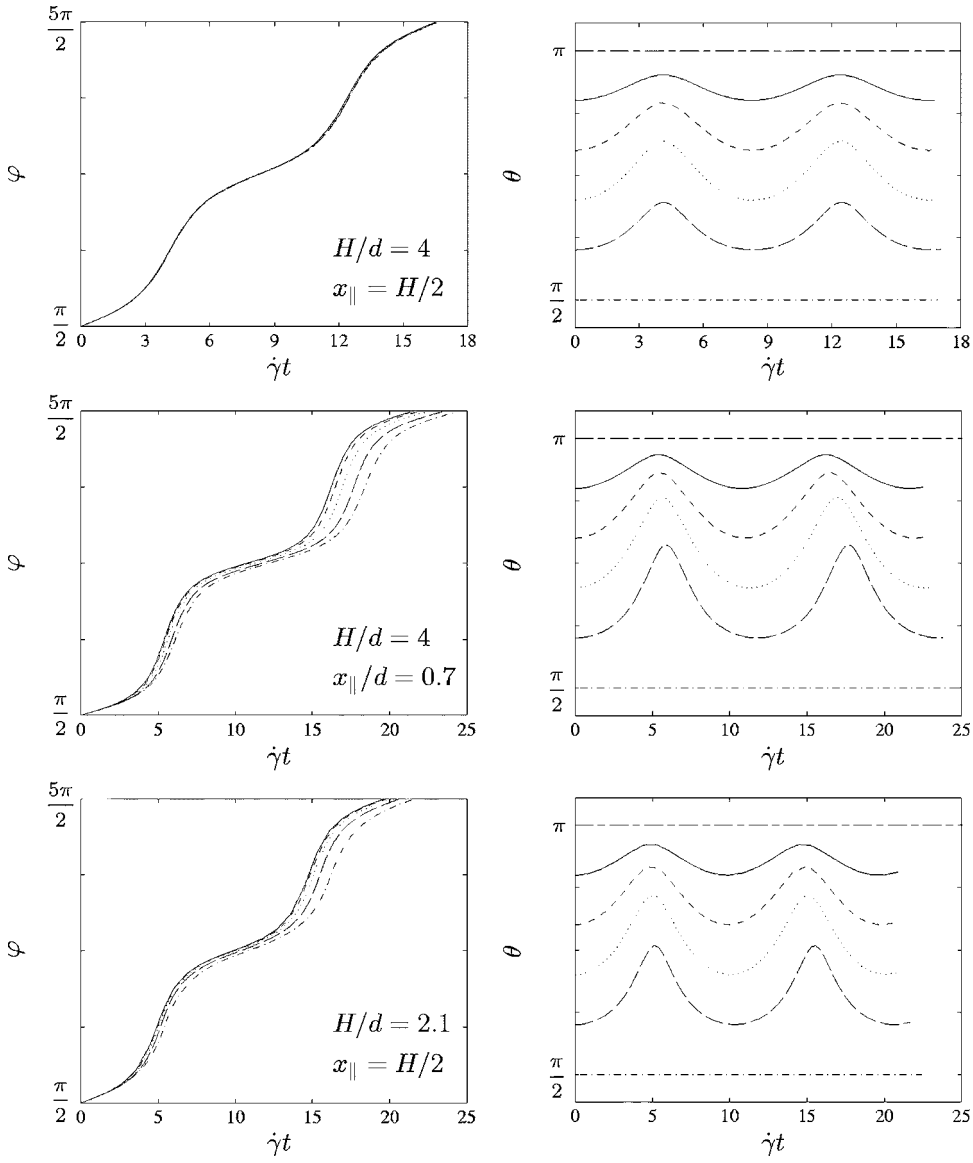

FIG. 4. Evolution of the orientation angles φ and θ for dumbbells undergoing periodic motion in shear flow between two parallel walls. The dumbbells are initially in the flow-vorticity plane $\varphi = \pi/2$. The wall separation H and initial position of particle center $x_\parallel$ are indicated in the left panels. Different lines correspond to different initial particle orientations $\theta_\parallel$ with respect to the vorticity axis (as specified in the right panels).

The results in the top two panels of Fig. 4 illustrate particle behavior under moderate-confinement conditions: the center of mass of the particle is in the midplane $x = H/2$ in a channel of moderate width $H/d = 4$. The results indicate that particle trajectories are qualitatively similar to Jeffery orbits in free space [Kim and Karrila (1991)]. In particular, all trajectories have approximately the same period T. Moreover, the evolution of the azimuthal angle φ is nearly independent of the initial orientation $\theta_\parallel$. When the particle is

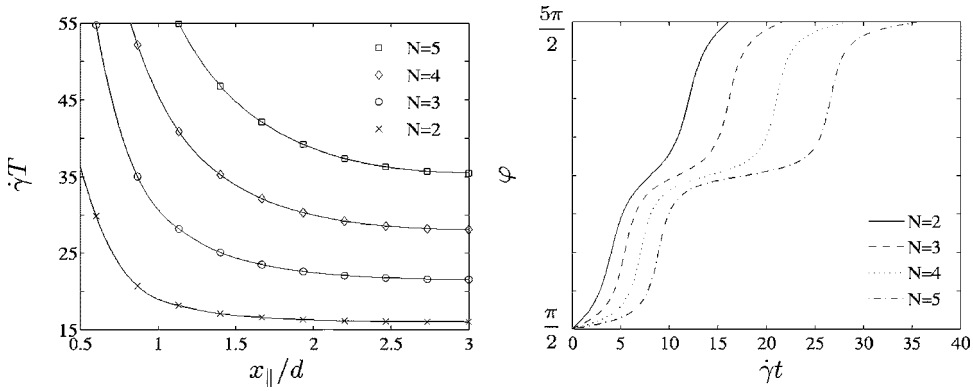

FIG. 5. Normalized period of motion $\dot{\gamma}T$ (left panel) and evolution of azimuthal angle ϕ (right panel) for chains of different length N, undergoing tumbling motion in shear flow in a channel with wall separation $H/d=6$. The chains are initially aligned with the flow and move in the plane $\theta=\pi/2$. The results in the left panel are plotted versus normalized initial position of the chain center $x_\parallel/d$; the selected trajectories shown in the right panel correspond to $x_\parallel=H/2$.

close to one of the walls (middle panels), or for a smaller wall separation (bottom panels of Fig. 4), the periods of particle motion become longer, and depend (although weakly) on the initial particle orientation.[1]

The dependence of the period T on particle position with respect to the walls for different chain lengths N is depicted in the left panel of Fig. 5 for a fixed channel width $H/d=6$. The results are plotted versus the position of the center of mass $x_\parallel$ of a chain when it passes the horizontal plane $\varphi=\pi/2$ during the tumbling motion. The results show that the period increases approximately linearly with the chain length, primarily due to the longer residence time in near-horizontal orientations (as depicted in the plot of the azimuthal angle φ versus time in the right panel of Fig. 5). This behavior is characteristic of Jeffery orbits in free space as well. Similar plots for different distances of the particle from the walls indicate that the increase of the period at small particle-wall separations (as seen in the left panel of Fig. 5) is also associated with the longer time that the particle spends oriented parallel to the walls.

For an axisymmetric particle in an unbounded shear flow, all particle trajectories can be parameterized by a single angle $\theta_\parallel$ that describes particle orientation with respect to the vorticity axis z when the particle crosses the flow-vorticity plane. However, in a wall-bounded system one needs to specify the corresponding position of the particle center of mass $x_\parallel$ as well. In addition to the configurational parameters $\theta_\parallel$ and $x_\parallel$, we also have two geometrical parameters: the chain length N and wall separation H. Since the number of parameters is large, we will not provide a complete characterization of the trajectories. Instead, in Fig. 6 we summarize our results by presenting the probability density for particle periods in a suspension of initially randomly distributed particles.[2]

The results in the left panel of Fig. 6 show the period distributions for dumbbells in channels with different values of the wall separation H/d. The results in the right panel

[1]We note that for an elipsoidal particle in shear flow bounded by a single wall similar results have been found by Pozrikidis (2005).

[2]Note that the vorticity component of the angular velocity Ω_z is positive for all particle configurations, according to our numerical results. Using the symmetries of the system one can thus show that all particle trajectories are periodic.

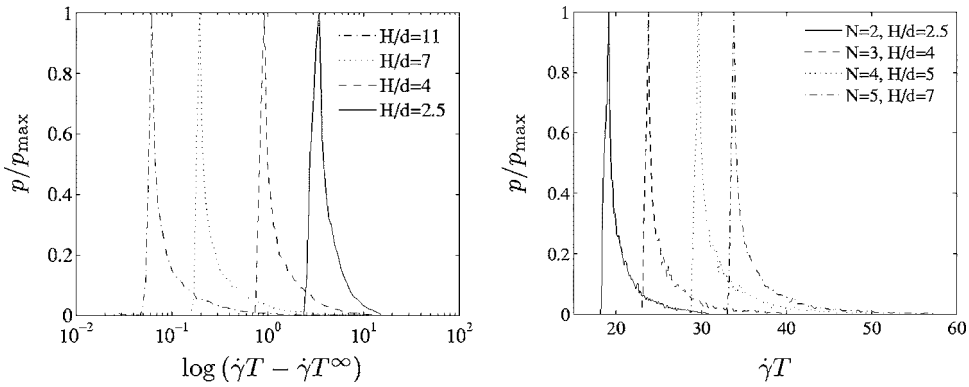

FIG. 6. Probability distribution $p(T)$ of particle periods T for chains with initial random distribution ρ^{eq}. Results correspond to dumbbells in systems with different wall separations H/d (left panel) and to chains of different length at a similar degree of confinement $H/(Nd)$ (right panel). Distribution p is normalized by its maximal value $p_{\max}$. In the left panel, $p(T)$ is shown versus logarithm of the period T shifted by the free-space value T^{∞}.

are for chains with different lengths in channels with a similar width-to-particle-lengths ratios $H/(Nd)$. In all cases, the period distributions are sharply peaked around the values corresponding to the particle in the center position, $x=H/2$. The distributions quickly ramp up, but they are not discontinuous. The results in the left panel (note the logarithmic scale) show that the distribution is broader for stronger confinements, i.e., for smaller values of $H/(Nd)$. This behavior is characteristic not only of dumbbells but it also holds for longer particles.

B. Evolution of the particle-wall gap

The center of mass of an axisymmetric particle moving in an unbounded shear flow translates with a constant velocity that is equal to the local value of the applied flow (1). In the wall-bounded shear flow, however, there is a significant coupling between the rotational and translational motion of the particle. This coupling is especially relevant for particles that are close to a wall because for such configurations the gap between the wall and particle surface may become extremely small at some portions of the particle trajectory.

This behavior is illustrated in Fig. 7, where the time evolution of the center of mass, orientation, and the dimensionless gap between the particle surface and the wall is depicted for a chain of $N=4$ spheres in a channel of width $H/d=6$. The particle-wall gap $\epsilon=\bar{x}/d-\frac{1}{2}$ (where $\bar{x}$ is the vertical position of the sphere in the chain that is closest to the lower boundary) is normalized by the particle diameter d. The particle is initially in the horizontal plane y-z, at a distance $x_{\|}/d=1.2$ from the lower wall. The results indicate that the minimal gap value $\epsilon_{\min}$ along the trajectory strongly depends on the initial particle orientation $\theta_{\|}$ (cf. the last panel in the figure). For particles approximately aligned with the vorticity direction (i.e., for $\theta_{\|}\approx 0$) the minimal gap is of the same order as the initial gap. In contrast, $\epsilon_{\min}$ is very small for particles rotating near the flow-gradient plane (i.e., for $\theta_{\|}\approx \pi/2$). This behavior is also evident in Fig. 8, where the minimal gap $\epsilon_{\min}$ is plotted versus $\theta_{\|}$ for different initial particle distances from the wall, $x_{\|}$ (left panel) and different particle lengths, N (right panel).

According to the results in Fig. 7, the gap decreases rapidly when the orientation vector $\mathbf{p}$ approaches the vertical plane perpendicular to the flow direction during the tumbling motion of the particle (i.e., when the azimuthal angle φ approaches π). At the

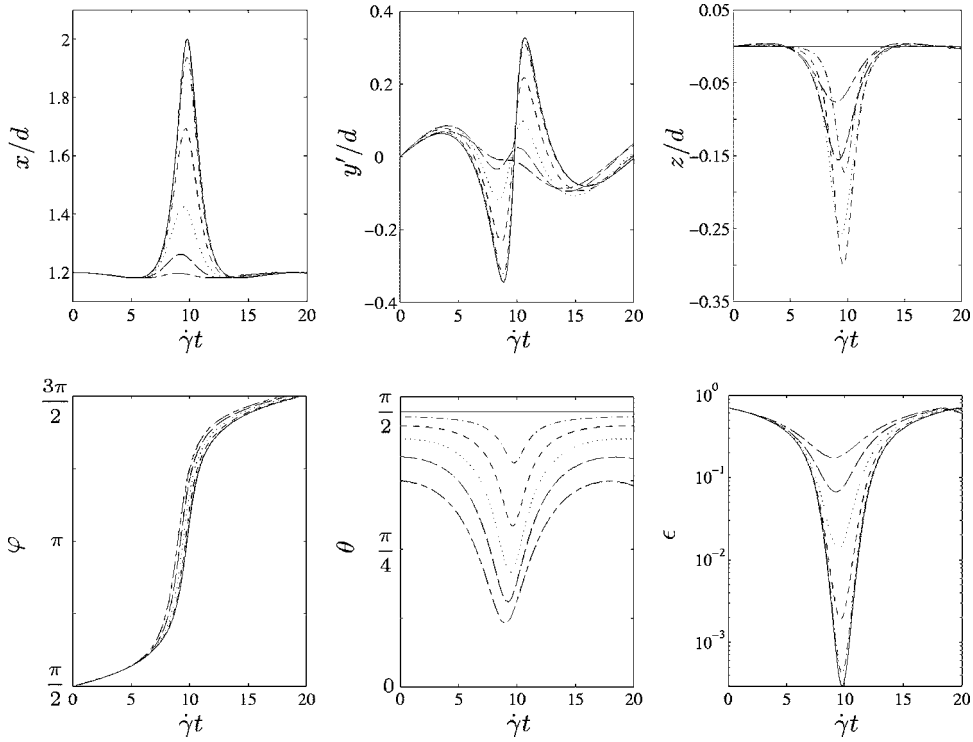

FIG. 7. Evolution of the center of mass (x, y', z), orientation (θ, ϕ), and dimensionless gap ϵ between particle surface and the lower wall, for a chain of length $N=4$, in a channel of width $H/d=6$. The chain is initially placed horizontally at $x_\parallel/d=1.2$. Different lines correspond to different initial orientations $\theta_\parallel$ with respect to the vorticity axis (as indicated in the bottom middle panel). The coordinate y' represents the y component of particle position measured in the coordinate system moving with the mean particle velocity. The results are shown over half-period $0<t<T/2$.

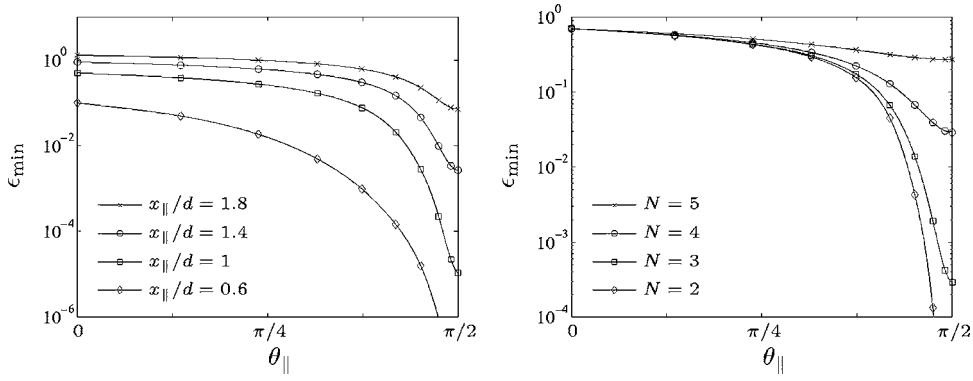

FIG. 8. Minimal value $\epsilon_{\min}$ (along the particle trajectory) of the dimensionless gap between the particle surface and the lower wall, for chains initially oriented in the flow-vorticity plane $\phi=\pi/2$ in a channel with wall separation $H/d=6$. The results are plotted versus initial particle orientation $\theta_\parallel$ with respect to the vorticity axis, for $N=4$ and several initial particle positions (left panel), and for $x_\parallel/d=1.2$ and several chain lengths (right panel).

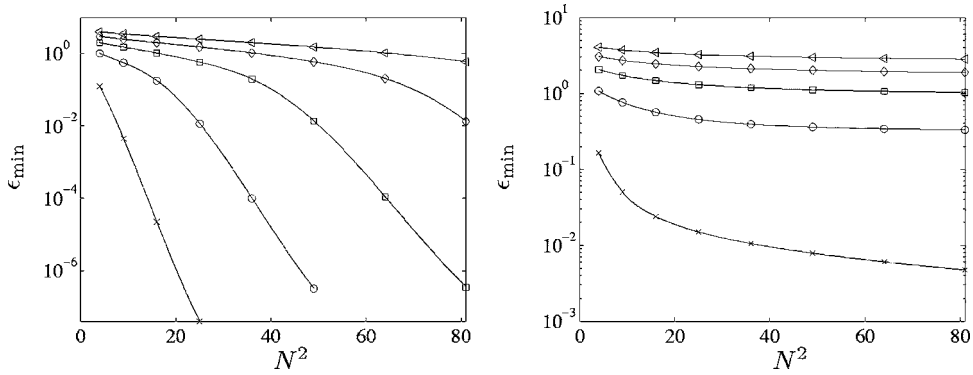

FIG. 9. Minimal value $\epsilon_{\min}$ of the dimensionless gap between the particle surface and the lower wall along the particle trajectory, for chains initially oriented in the flow-vorticity plane $\phi=\pi/2$ in a channel with wall separation $H/d=100$. The results are plotted versus chain length squared, N^2, for the initial particle positions, from top to bottom, $x_{\|}/d=5,4,3,2,1$. Particle initially aligned with the flow (left panel); particle initial orientation $\theta_{\|}-\pi/2=15°$ (right panel).

same time, the vertical coordinate of the particle center increases rapidly. A similar "pole vault" particle motion was observed by Mody and King (2005) in their study of an oblate particle in shear flow close to a single wall. Such motion was also seen in recent experiments [Moses *et al.* (2001), and references therein].

For some particle configurations, especially for long chains initially aligned with the flow at a small distance from the wall, the minimal particle-wall gap may become orders of magnitude smaller than the particle diameter d. These unphysically small gaps are associated with the exponential drainage of the lubrication layer that separates the nearly touching chain end from the wall. The rapid drainage is produced by the slowly varying hydrodynamic pushing force that acts on the outer portions of the particle. Since the spheres in the chain cannot freely move due to the rigid-body constraints, a typical sphere translates with a velocity $\sim N\dot{\gamma}d$ with respect to the fluid. This relative motion produces a hydrodynamic resistance force proportional to the chain length N. The resistance force acts on all N spheres in the chain. Thus, the total force pushing the chain towards the wall before the particle crosses the vertical plane is approximately proportional to N^2. We note that there is a finite normal force component, because the spheres move away from the wall due to the rotation of the chain with respect to the near-contact point.

Assuming a nearly constant drainage time $\tau\sim\dot{\gamma}^{-1}$, which corresponds to the time the particle spends rotating towards the vertical plain $\varphi=0$,[3] we find that the minimal gap decays as

$$\epsilon_{\min}\sim\exp(-\alpha N^2) \tag{12}$$

with the chain length N for $N\gg 1$. To obtain this result, we have used the linear dependence of the lubrication mobility on the particle-wall gap ϵ [Cichocki and Jones (1998); Kim and Karrila (1991)].

The result (12) is confirmed by the data presented in Fig. 9. Our detailed calculations

[3]Indeed, the drainage time may increase logarithmically with the minimal gap, because particle rotation around the contact point is hindered by the logarithmic lubrication resistance. However, such hindrance of particle rotation has a significant effect only at extremely small gaps. Moreover, the effect of increased drainage time should be compensated by the weaker pushing force due to slower rotation of the chain (and thus smaller normal velocities of the individual spheres).

show that the coefficient α (corresponding to the slope of the curves in Fig. 9 for large N) has a sharp maximum at $\theta_{\|}=\pi/2$. However, when the particle is misaligned with the flow-gradient plane $\theta_{\|}=\pi/2$ even by as little as 15°, α is significantly smaller, as seen in the right panel of Fig. 9. Some important consequences of this observation are discussed in the following section.

C. Significance of particle-wall collisions

The unphysically small particle-wall gaps that are predicted for some initial particle configurations indicate that a suspension of nonspherical particles undergoing shear flow in a wall-bounded system cannot be fully characterized by hydrodynamic considerations alone. An appropriate description of the near-contact particle-wall interactions is also necessary. Under some conditions, for example, particles with trajectories resulting in very small gaps may get into mechanical contact with the walls due to roughness. In other systems, a sufficiently strong repulsive interparticle potential (e.g., screened Coulombic repulsion) may prevent further drainage of the particle-wall gap. The development of unphysically small gaps could also be hindered by Brownian motion even if the Peclet number based on particle size is quite large.[4]

It is thus important to determine if the near-contact interactions affect the quantities of interest for a specific problem. For some processes, such as particle deposition and resuspension, the near-contact interactions cannot be ignored because they significantly affect the particle behavior. However, as shown below, particle-wall collisions have only a small effect on the rheological response of the suspension, provided that $H>Nd$ and the chains are not too long.

To demonstrate the validity of this statement, we first examine the evolution of the stresslet induced on the particles whose trajectories were shown in Fig. 7. The behavior of the shear component of the stresslet S_{xy} is displayed in the top panel of Fig. 10, and the behavior of the normal-stress components

$$S_1 = S_{yy} - S_{xx}, \quad S_2 = S_{xx} - S_{zz}, \tag{13}$$

is shown in the bottom panels. These components contribute to the effective shear stress and the normal-stress differences in suspension flow, according to the discussion in Sec. V. The stresslet of the chain is normalized by the shear component (10) of the stresslet induced on a sphere subject to shear flow with the same strength $\dot{\gamma}$ in free space.

According to the results in Fig. 10, all three stresslet components exhibit large peaks for those particle configurations for which very small gaps develop (i.e., for particles that are rotating near the flow-gradient plane). For the shear component of the stresslet we also show, in the inset (top right), the peak, average, and minimal values of S_{xy} along the trajectory versus the initial orientation $\theta_{\|}$. For the normal-stress components (13) the insets present only peak values because the time average vanishes, due to symmetry. Since each of the N spheres in the chain is subject to $O(N)$ hydrodynamic stresses, we expect that peak values scale as N^2 with the chain length.

To determine how strongly the trajectories with very small particle-wall gaps may affect the shear-stress response of a bounded suspension, we note that the time average of S_{xy} for such trajectories differs by a relatively small factor from typical values for orbits

[4]By comparing the magnitudes of thermal and hydrodynamic forces one can estimate that Brownian motion is important in the near-contact boundary layer of thickness $\epsilon \sim N\mathrm{Pe}^{-1}$, where $\mathrm{Pe}=l^3\eta\dot{\gamma}/(kT)$ is the Peclet number based on the chain length $l=Nd$, and kT is the thermal energy. We note that weak Brownian motion may also affect the period of motion for long chains by moving the chains out of alignment with the flow-vorticity plane where they would otherwise spend a much longer time [Leal and Hinch (1971)].

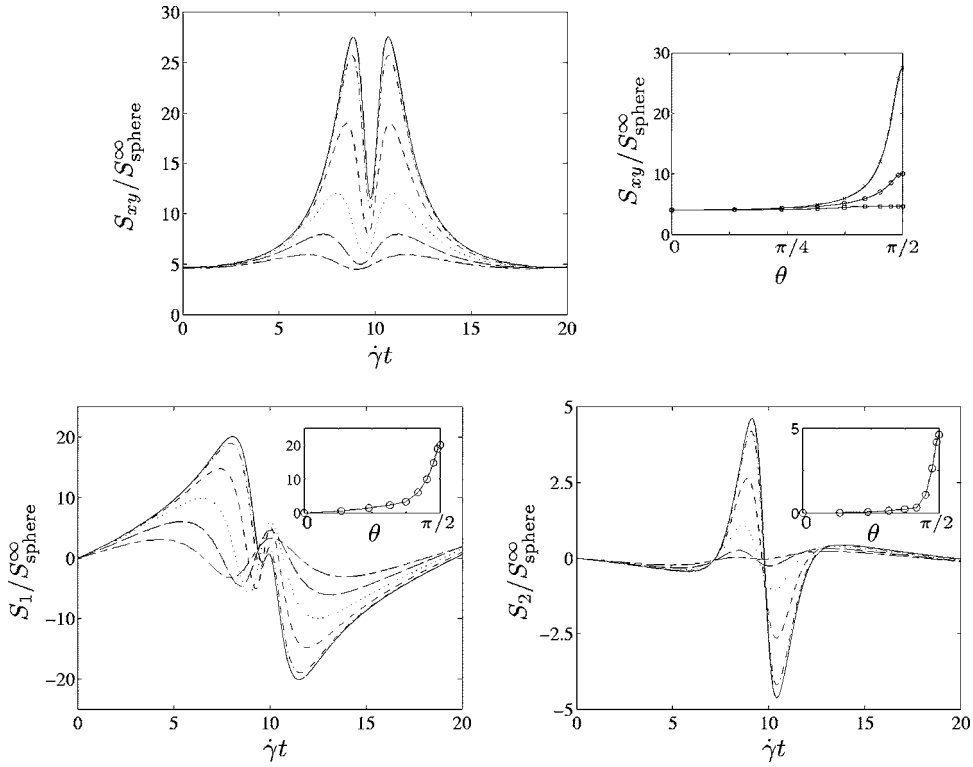

FIG. 10. Evolution over half-period of the shear component S_{xy} and normal-stress components S_1 and S_2 [as defined by Eq. (13)] for the stresslet induced on a chain of length $N=4$, initially located at $x_{\parallel}/d=1.2$ in a channel of width $H/d=6$. Different lines correspond to different angles $\theta_{\parallel}$, as defined by the line type used in Fig. 7. Insets show the minimal, maximal, and average values for the shear component S_{xy}, and the maximal values for the normal-stress components S_1 and S_2.

that do not lead to particle-wall collisions. For example, the time average of the normalized stresslet on the trajectories illustrated in Fig. 10 does not exceed $S_{xy}/S^{\infty}_{\text{sphere}} \approx 10$. This value should be compared with the average value $\langle S_{xy}\rangle/S^{\infty}_{\text{sphere}} \approx 6$ for the whole ensemble of the trajectories in this system (cf. Fig. 18 in Sec. V C below). For normal-stress components we obtain a similar conclusion, except that the amplitude of oscillations should now be considered instead of the time averages (which vanish).

As we have already observed in Sec. IV B, the near-contact trajectories require that the particle be both close to the wall and rotate close to the flow-gradient plane. The configuration-space volume corresponding to such trajectories is thus small, and, therefore, they occur infrequently (the frequency $\lesssim 3\%$ for $H/d \gtrsim N$ and $N \leq 5$, according to the results shown in Fig. 11). The corresponding contribution to the effective stress (7) can thus be neglected without introducing significant inaccuracies, provided that the chain length N is moderate and the wall separation H larger than the particle length Nd.

In this paper we focus on systems where the effects of near-contact nonhydrodynamic interactions are negligible, and, therefore, the moderate-confinement condition $H/d > N$ is assumed. It is thus important to determine how crucial this condition is. To this end, in Fig. 12, we show the evolution of the particle orientation, particle-wall gap, and three stresslet components S_{xy}, S_1, and S_2, for a system with $N=4$ and $H/d=3$. The particle center is in the midplane $x=H/2$, so that the two gaps between the walls and the particle

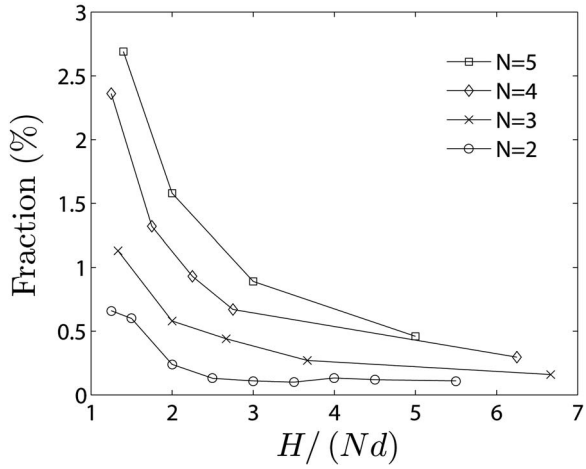

FIG. 11. Fraction (in percent) of trajectories with minimal gap $\epsilon_{\min} < 10^{-3}$ for a system of chains with initial random distribution ρ^{eq} versus degree of confinement $H/(Nd)$ for several values of chain length N.

surface are the same. The results of our simulations indicate that for particles oriented near the flow-gradient plane $\theta = \pi/2$ the gaps ϵ decay very rapidly. They achieve values below 10^{-8} before the vertical particle position with $\phi = 0$ is reached. (We stop our

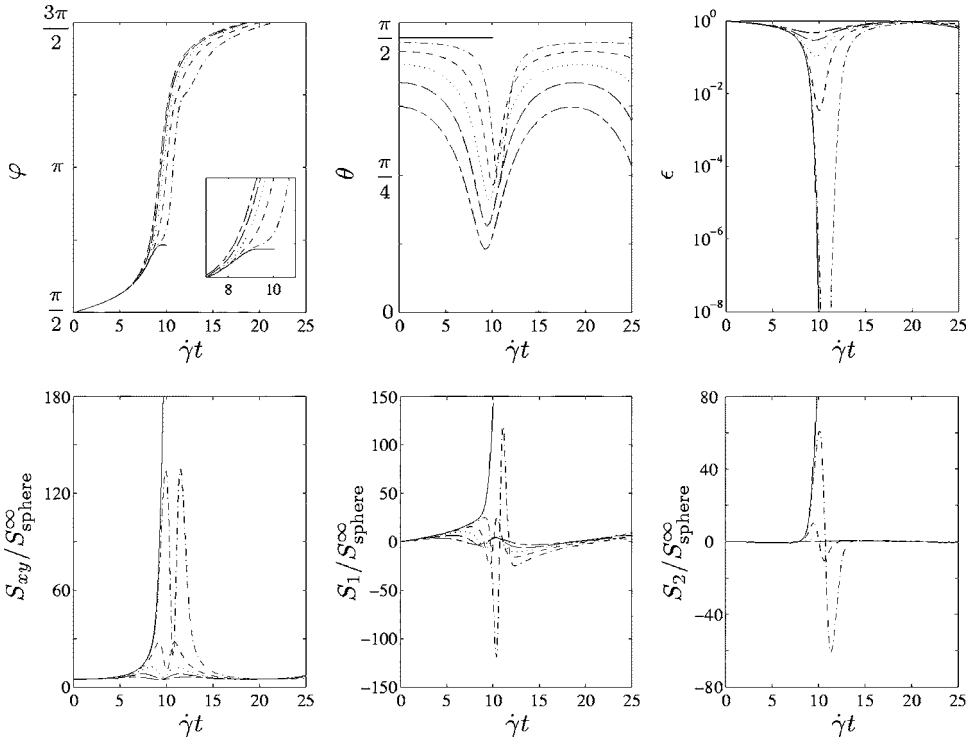

FIG. 12. Evolution over half-period of the orientation angles φ and θ, gap ϵ, and normalized stresslet components S_{xy}, S_1, and S_2 of a chain with length $N=4$ and the center of mass in the midplane of a channel with wall separation $H/d=3$. Different lines correspond to different initial angles $\theta_{\|}$, as defined in the top middle panel.

simulation for $\epsilon = 10^{-10}$.) The rapid decrease of the gaps is accompanied by a sharp increase of the shear and normal components of the stresslet. For a particle rotating in the plane $\theta = \pi/2$ all components diverge, and for $|\theta - \pi/2| \ll 1$, the stresslets achieve peak values that are much higher than the ones observed for $H/d > N$ (as illustrated in Fig. 10).

The marked difference in the particle behavior for $H/d < N$ and $H/d > N$ stems from the interaction between two particle-wall lubrication layers in the strongly confined case $H/d < N$. By analyzing the effects of the normal and tangential forces in two lubrication regions coupled via the rigid-body constraint, we find that the particle-wall gaps decrease as $\epsilon \sim \exp[-\exp(\alpha t)]$ for trajectories with $\theta_{\|} \approx \pi/2$. This explains why the gaps decrease so rapidly. The corresponding increase of the stresslet components is exponential due to the logarithmic behavior of the tangential lubrication force. The sharp decrease of the gaps and the corresponding large values of the stress contributions indicate that for strongly confined systems with $H/d < N$ the effect of direct particle-wall interactions on the rheological response of the suspension cannot be ignored.

We conclude this section with a comment that the near-contact particle behavior is not merely an algorithmic problem. The near contact particle-wall interactions do physically occur in real systems. It is thus crucial to determine under what conditions such interactions significantly affect the behavior of the system (in which case a specific near-contact-interaction model needs to be specified), and under what circumstances the effect of such interactions can be neglected. This remark applies not only to our present problem, but also to flowing suspensions in general.

V. RHEOLOGY OF DILUTE SUSPENSION OF LINEAR CHAINS

We now investigate the rheological response of a dilute suspension of noninteracting linear chains of spheres to a sudden onset of shear flow in a wall bounded system. As discussed in Sec. II C, we assume that the initial state of the suspension is characterized by the equilibrium particle distribution. The flow distorts the initial distribution, which leads to nontrivial rheological behavior.

We focus on configurations with $H/d > N$ and moderately long chains $N \leq 5$. Under these conditions the near-contact particle trajectories do not affect the suspension rheological response (cf. the discussion in Sec. IV C). In our numerical simulations we thus neglect trajectories with $\epsilon_{\min} \leq 10^{-5}$ without introducing any significant inaccuracies. As illustrated in Fig. 18 (see Sec. V C below), our results are insensitive to the gap-truncation value.

A. Shear stress and normal-stress differences

In the absence of Brownian motion and other nonhydrodynamic relaxation mechanisms, the effective stress (6) in a sheared suspension is proportional to the shear rate $\dot{\gamma}$. As in unbounded space, the rheological response of the system is characterized by the effective shear stress σ_{xy}^{eff} and the normal stress differences

$$N_1 = \sigma_{yy}^{\text{eff}} - \sigma_{xx}^{\text{eff}}, \quad N_2 = \sigma_{xx}^{\text{eff}} - \sigma_{zz}^{\text{eff}}. \tag{14}$$

According to Eqs. (6) and (7), the shear stress consists of a background-fluid contribution and a particle contribution,

$$\sigma_{xy}^{\text{eff}} = 2\eta E + \sigma'_{xy}, \tag{15}$$

where

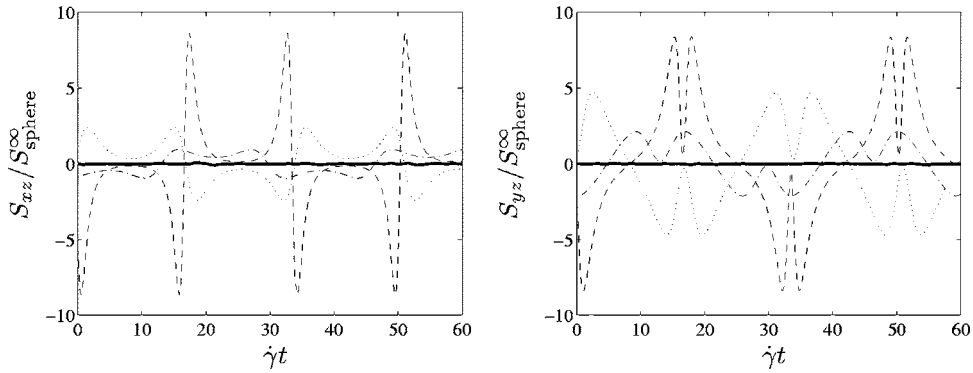

FIG. 13. Evolution of the normalized stresslet components S_{xz} and S_{yz} for three randomly chosen trajectories of chains with lengths $N=5$ in a channel with wall separation $H/d=7$ (broken lines). The average values $\langle S_{xz}\rangle$ and $\langle S_{yz}\rangle$ for a system of chains with initial random distribution ρ^{eq} vanish, as indicated by the solid lines. Due to symmetry, the time averages of individual contributions S_{xz} and S_{yz} also vanish.

$$\sigma'_{xy} = n_{\text{p}}\langle S_{xy}\rangle. \tag{16}$$

The normal stress differences have only the particle contributions

$$N_i = n_{\text{p}}\langle S_i\rangle, \quad i=1,2, \tag{17}$$

where the stresslet components S_i are defined by Eq. (13). The remaining components of the effective stress tensor σ^{eff}_{xz} and σ^{eff}_{yz} vanish owing to the flow geometry and the statistical symmetry of the particle ensemble with respect to the reflection of the vorticity axis z. We note, however, that the unaveraged stresslet components S_{xz} and S_{yz} are nonzero on typical trajectories, as illustrated in Fig. 13.

In what follows, particle contributions to the shear stress and normal stress differences in a suspension of chains are shown normalized by the particle contribution to the shear-stress in an unbounded suspension of spheres with the same number density n_p (and thus volume fraction smaller by the factor of N), undergoing shear flow of the same strength $\dot{\gamma}$. Accordingly, we show the quantities

$$\frac{\sigma'_{xy}}{n_p S^{\infty}_{\text{sphere}}} = \frac{\langle S_{xy}\rangle}{S^{\infty}_{\text{sphere}}} \tag{18}$$

and

$$\frac{N_i}{n_p S^{\infty}_{\text{sphere}}} = \frac{\langle S_i\rangle}{S^{\infty}_{\text{sphere}}}, \quad i=1,2, \tag{19}$$

where $S^{\infty}_{\text{sphere}}$ is given by Eq. (10). The results of our simulations, presented in Figs. 14–19 were obtained from ensemble averages over up to 10^4 trajectories.

B. Time-dependent rheological response to a sudden onset of shear flow

We begin our analysis by discussing the evolution of the shear stress for a system of noninteracting linear chains of spheres undergoing shear flow in unbounded space. We recall that the motion of axisymmetric particles in unbounded shear flow is periodic, with a period which is independent of the initial orientation of the particle [Bretherton (1962), Jeffery (1922)]. Thus, the ensemble-averaged stress response of a dilute, monodisperse suspension to such a flow is also periodic.

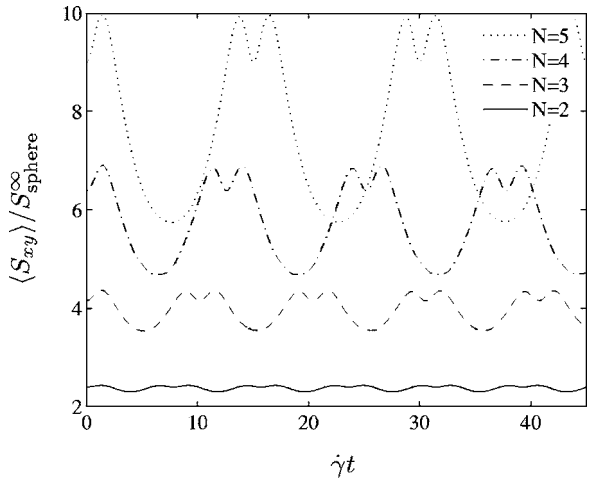

FIG. 14. Evolution of the normalized particle contribution to shear stress (18) in an unbounded, dilute suspension of linear chains of spheres with initial random distribution ρ^{eq}, after the onset of steady shear flow. Different lines correspond to different chain lengths N.

This behavior is illustrated in Fig. 14, where the time evolution of the normalized particle contribution to the shear stress (18) is plotted for several chain lengths N. The results show that the stress response undergoes pronounced oscillations, especially for large values of N. Time-average values of the normalized shear-stress contribution $\langle S_{xy}\rangle / S^{H}_{\text{sphere}}$ and the period of the oscillations T also increase with N. This behavior is consistent with our discussion of individual particle trajectories in Sec. IV. The characteristic "dimpled" shape of the stress-response curves results primarily from the contributions of the chains moving near the flow-gradient plane. Due to the symmetry of the problem, these shear-stress contributions achieve maximal values at azimuthal angles $\varphi = \pi/4$ and $3\pi/4$, and have a deep minimum for $\varphi = \pi/2$. This behavior is seen, for example, in the top panel of Fig. 10 for a particle whose trajectory is represented in Fig. 7.

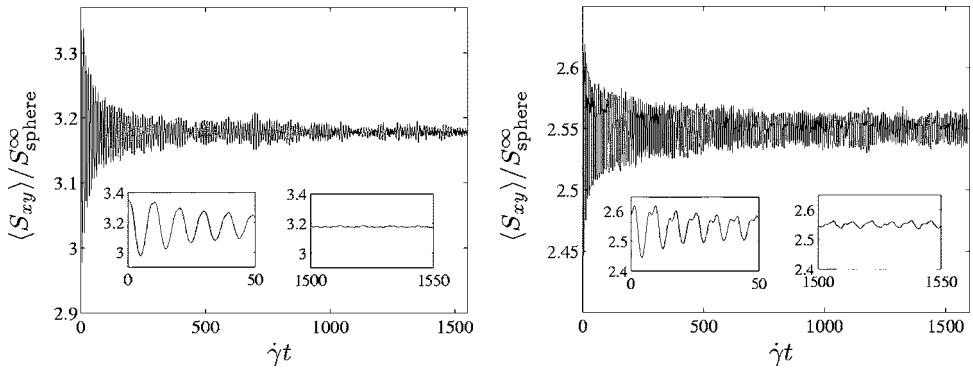

FIG. 15. Evolution of the normalized particle contribution to shear stress (18) in a dilute suspension of dumbbells with random initial distribution ρ^{eq}, after onset of steady shear flow in a channel with wall separation $H/d=2.5$ (left panel) and $H/d=7$ (right panel). Insets show details of the shear-stress behavior at the onset of the flow and after long times. Weaker confinement (greater H/d) results in a much slower approach to steady state.

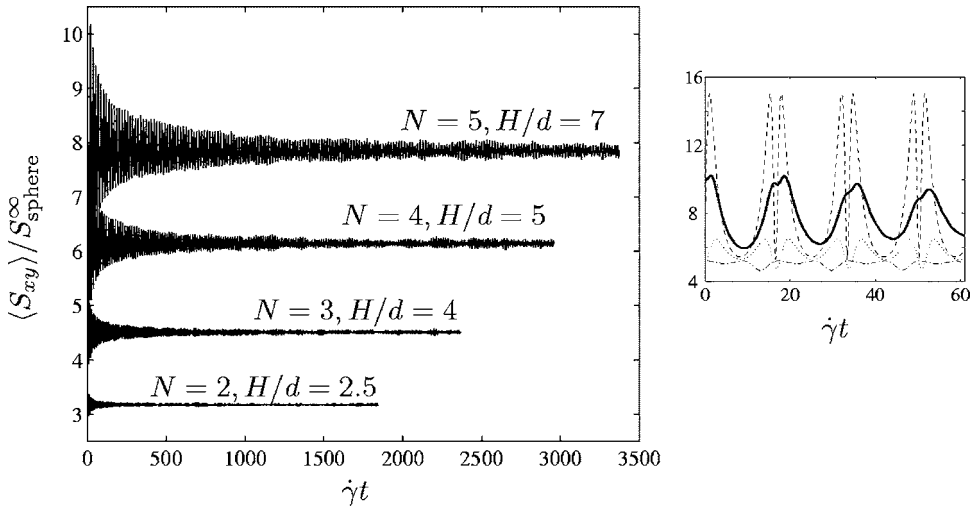

FIG. 16. Same as Fig. 15, except that results are for chains with different lengths N in channels with similar values of wall separation normalized by particle lengths $H/(Nd)$. Inset shows details of the initial behavior of the ensemble-averaged shear stress (18) at the onset of the flow (solid line) and three randomly chosen individual particle contributions (broken lines) for N=5 and H/d=7.

In the absence of Brownian motion or other relaxation mechanisms (such as interparticle hydrodynamic interactions at finite suspension concentrations) the stress oscillations in an unbounded suspension do not relax. In the presence of walls, however, we observe decaying oscillations, as illustrated in Figs. 15 and 16 for the shear stress and Fig. 17 for the normal stress differences. The decay of the oscillations is associated with the phase shifts resulting from the continuous distribution of the periods of particle orbits, as discussed in Sec. IV and shown in Fig. 6.

Figure 15 represents the shear-stress evolution in a suspension of noninteracting dumbbells (N=2) for two values of the wall separation H/d=2.5 and H/d=7. In both cases, the oscillations first decay relatively rapidly. At longer times, however, a much

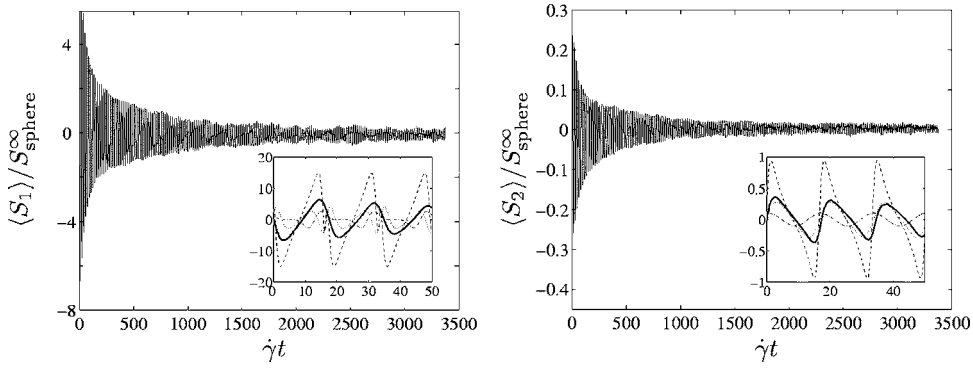

FIG. 17. Evolution of the normalized particle contributions to the first (left panel) and second (right panel) normal stress differences (19) in a dilute suspension of chains of length N=5 after the onset of a steady shear flow in a channel with wall separation H/d=7. Inset shows details of the initial behavior of the ensemble-averaged normal stress differences (19) (solid line) and three randomly chosen individual particle contributions (broken lines).

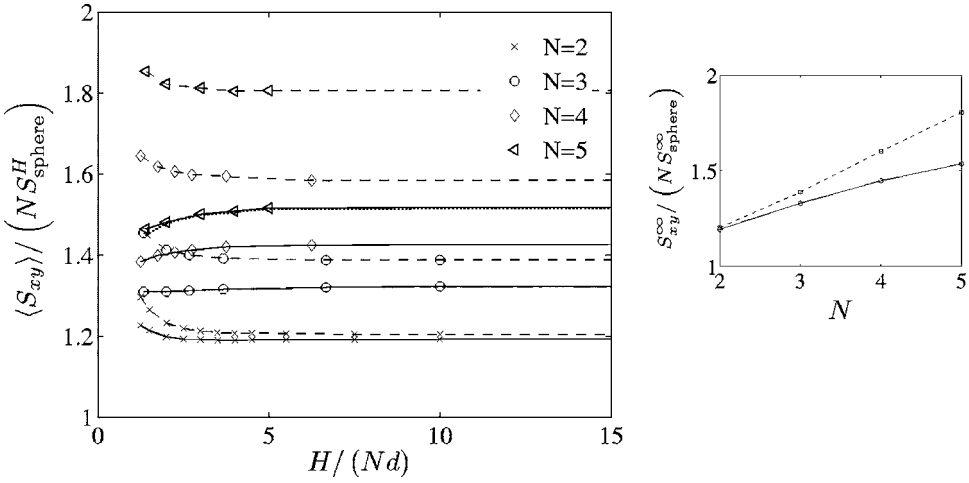

FIG. 18. Short-time (dashed lines) and long time (solid lines) values of the normalized particle contribution to the shear stress (20) in a dilute suspension of chains of length N with random initial distribution ρ^{eq}, after the onset of a steady shear flow between parallel walls, versus the degree of confinement $H/(Nd)$. The dotted line, nearly overlapping with the solid line for $N=5$, represents the corresponding approximate long time results obtained by neglecting trajectories for which the minimal particle-wall gap $\epsilon_{\text{min}} < 10^{-3}$ (other long-time results include contributions from all trajectories with $\epsilon_{\text{min}} > 10^{-5}$). The inset shows the low-confinement limits $H/(Nd) \to \infty$ of the shear stress versus the chain length N.

slower relaxation is seen. This slow decay is associated with the sharp peak of the period distribution shown in the left panel of Fig. 6. The peak is much narrower for the larger wall separation, so the oscillations decay much more slowly for $H/d=7$ than for $H/d=2.5$. For the larger value of H/d the oscillations are still present even for $\dot{\gamma}t \approx 10^3$. In contrast, for the smaller value only statistical noise is observed at such a long time.

Figure 16 shows that the same qualitative behavior applies not only to dumbbells, but also to longer chains. In this figure, the particle contribution to the shear stress is plotted versus time for chains of lengths $N=2,\ldots,5$, in systems with a similar degree of confinement H/d. The corresponding period distributions are presented in the right panel of

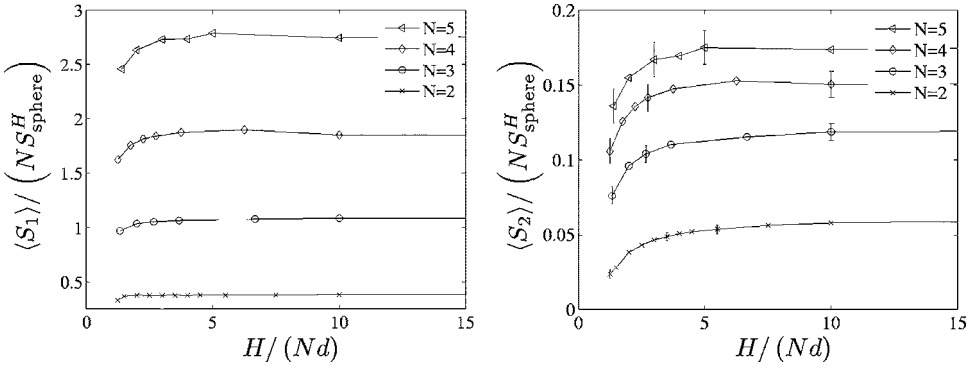

FIG. 19. Initial oscillation amplitudes of the normalized first and second normal-stress differences (21) in a dilute suspension of chains of length N with random initial distribution ρ^{eq}, after the onset of a steady shear flow between parallel walls, versus the degree of confinement $H/(Nd)$. Error bars in the plot of the second normal-stress difference represent statistical uncertainty defined as one standard deviation. Statistical inaccuracies of the first normal-stress difference are much smaller.

Fig. 6. In all the cases considered, the oscillations of the shear stress decrease in time, and the system finally reaches a steady state. The relaxation time is longer for longer chains, because a typical period of a particle trajectory is longer for greater N according to the results shown in the right panel of Fig. 6. (We note, however, that the width of the period distributions is similar for all systems represented in the plot.)

The evolution of the normal-stress differences (19), depicted in Fig. 17 for $N=5$ and $H/d=7$, has many features similar to the evolution of the shear stress, discussed above. Both $\langle S_1 \rangle$ and $\langle S_2 \rangle$ exhibit slowly decaying oscillations. However, in contrast to $\langle S_{xy} \rangle$, normal stress differences oscillate around zero mean values because the time averages of $\langle S_1 \rangle$ and $\langle S_2 \rangle$ vanish at each trajectory due to the flow-reflection symmetry. Moreover, $\langle S_1 \rangle = \langle S_2 \rangle = 0$ at $t=0$ because of the flow-reflection symmetry of Stokes flow and the reflection symmetry of the initial random distributions of chains.

We note that for a smooth distribution of periods of individual trajectories, the oscillations of the shear stress and normal stress differences would decay as t^{-1} (this can be shown by estimating the fraction of trajectories for which a sufficient phase shift occurred at a given time to randomize their contribution to the ensemble-averaged stress). The oscillations seen in Figs. 14–17, however, decay more slowly because of the sharp peak of the period distribution depicted in Fig. 6.

C. Results for different chain lengths and degrees of confinement

We conclude our analysis by summarizing, in Figs. 18 and 19, the results of a series of numerical simulations for systems with different channel widths and for chains of different lengths. Figure 18 shows instantaneous short-time values ($t=0$) and long time values ($t \to \infty$) of the shear stress $\langle S_{xy} \rangle$. Since the relaxation of the ensemble-averaged stress occurs only through the phase shifts associated with different periods of particle trajectories, the long-time value of $\langle S_{xy} \rangle$ is equivalent to the time average of this quantity. Accordingly, the long-time values shown in Fig. 18 have been evaluated by time-averaging our numerical results.

Symmetry considerations presented in Sec. V B lead to the conclusion that normal stress differences $\langle S_1 \rangle$ and $\langle S_2 \rangle$ vanish for both $t=0$ and $t \to \infty$. In Fig. 19 we thus present the initial oscillation amplitudes for these stress components. (The amplitudes are evaluated as the difference between the maximal and minimal value.) The results in Figs. 18 and 19 are plotted for several chain lengths N versus the wall separation normalized by the length of the particles $H/(Nd)$.

To emphasize the dependence of the rheological response of the system on chain length, the stress components shown in Figs. 18 and 19 are normalized differently than the stresses represented in previous figures. Instead of dimensionless quantities (18) and (19) we plot

$$\frac{\sigma'_{xy}}{\tilde{n}_p S^H_{\text{sphere}}} = \frac{\langle S_{xy} \rangle}{N \langle S^H_{\text{sphere}} \rangle} \tag{20}$$

and

$$\frac{N_i}{\tilde{n}_p S^H_{\text{sphere}}} = \frac{\langle S_i \rangle}{N \langle S^H_{\text{sphere}} \rangle}, \quad i = 1,2, \tag{21}$$

where

$$\widetilde{n}_{\mathrm{p}} = N n_{\mathrm{p}} \tag{22}$$

is the number density of spheres in the system (rather than the number density of chains of spheres). The normalization factor $\langle S^H_{\mathrm{sphere}} \rangle$ in Eqs. (20) and (21) corresponds to the ensemble-averaged particle contribution to the shear stress in a suspension of spheres undergoing shear flow in a channel with the same width H as the suspension of chains. Our results for $\langle S^H_{\mathrm{sphere}} \rangle$ are given in the right panel of Fig. 3 and in Table I. According to the above definitions, the deviations of the quantities (20) and (21) from unity are associated with the rigid-body constraints that restrict the relative motion of spheres forming a chain.

The results in Figs. 18 and 19 indicate that the rescaled quantities (20) and (21) strongly depend on the chain length N. This dependence is nearly linear for the short-time value of the shear stress and for the first normal-stress difference N_1. For the long time value of the shear stress and for the second normal-stress difference N_2 a somewhat weaker dependence is observed. The nearly linear dependence of the stresses on the chain length N can be qualitatively explained using arguments similar to those leading to Eq. (12).

For longer chains, the long-time value of the shear stress is significantly smaller than the short time value because highly elongated particles are predominantly orientated in the flow-vorticity plane during their periodic motion (as illustrated in the right panel of Fig. 5). For a suspension of short chains, the nonisotropy associated with this dynamic orientation mechanism is relatively weak. Thus, for dumbbells the short- and long-time values are nearly the same. For similar reasons, the magnitude of the oscillations of the scaled normal stress differences (21) significantly increases with N. We note that the magnitude of $\langle S_1 \rangle$ is much larger than the magnitude of $\langle S_2 \rangle$, which is a frequently observed pattern.[5]

It is interesting to note that confinement only moderately affects the magnitudes of the shear stress and the normal-stress differences in our system. According to the results shown in Fig. 18, the initial shear-stress response increases with the decreasing channel width H. In contrast, the magnitude of the long-time response increases for dumbbells, but decreases for longer chains. Once again, this behavior is associated with the longer time the chains spend near the flow-vorticity plane—in narrow channels the chain rotation is hindered by the hydrodynamic interactions with the walls (cf. the discussion in Sec. IV A). Chains oriented in the flow-vorticity plane contribute to the stress less than chains with other orientations. A similar reduction of the magnitude of the stress when the channel width is decreased can be observed for the normal-stress differences shown in Fig. 19.

VI. CONCLUSIONS

We have presented a detailed analysis of the effects of confining walls on the dynamics of a dilute suspension of noninteracting, elongated axisymmetric particles undergoing a steady shear flow in a parallel-wall rheometer. We have investigated the effects of the walls on the trajectories of individual particles, the evolution of the stresslets induced on

[5]Since the second normal stress difference N_2 involves cancellation of many order-one contributions, the statistical uncertainties for this quantity (in Fig. 19 indicated by the error bars corresponding to one standard deviation) are quite large. The statistical uncertainties of the shear stress and the first normal stress difference, however, are much smaller.

the particles, and the resulting stress response of the system. Our numerical results have been obtained for particles modeled as linear chains of spheres, but the qualitative conclusions of our study also apply to other axisymmetric particles.

We have found that particle motion in the two-wall system qualitatively resembles the Jeffery's orbits in the unbounded space, provided that the wall separation is greater than the particle length. There are, however, important differences between the unbounded and confined systems. While in both geometries all particle trajectories are periodic (apart from the systematic translational motion in the flow direction), in wall-bounded systems the period of motion and the evolution of the azimuthal angle φ depend on the initial position and orientation of the particle. Especially, particles that are close to a wall remain oriented near the flow-vorticity plane (i.e., a plane parallel to the walls) significantly longer than the particles that are far from the walls. In contrast, in free space the period of motion and the evolution of the azimuthal angle are independent of the initial conditions.

Particles that are initially nearly aligned with the flow direction at a sufficiently small distance from a wall (less than half of the particle length) undergo a pole-vault motion during which the gap ϵ between the wall and one of the particle ends may become extremely small. {A similar motion has been earlier described for single-wall systems [Mody and King (2005), Moses *et al.* (2001)].} We have shown that for a given initial particle position the minimal gap ϵ decreases exponentially with the square of the particle length. Due to this exponential behavior, particle-wall gaps become unphysically small for some initial configurations, especially for strongly elongated particles. However, we have also shown that even a small misalignment of the particle with the flow-gradient plane significantly reduces this effect.

To determine the effect of "collisional" particle trajectories (i.e., trajectories resulting in very small gaps) on the rheological response of the system, we have performed computer simulations for an ensemble of particles with random initial configurations. We have found that unphysically small gaps occur only for a small fraction of particles, provided that the wall separation H is larger than the particle length l. Moreover, the contributions of collisional trajectories to the effective stress are negligible. Therefore, the rheological response of moderately confined suspensions with $H > l$ is insensitive to the system-dependent, short-range non-hydrodynamic force exerted by a wall on a particle when the gap ϵ becomes very small.

The near-contact particle-wall interactions are much more important at stronger confinements $H < l$. First, the fraction of the near-contact trajectories is significantly larger in such systems than in moderately confined suspensions. Moreover, the stresslet induced on a particle becomes very large when both ends of the particle are nearly touching the opposing walls. Thus, the effective-stress response strongly depends on the form of nonhydrodynamic near-contact forces. Under some conditions, for example, the fast decay of the particle-wall gaps may result in particle jamming (a phenomenon which by itself warrants a separate study). Since we are concerned here with purely hydrodynamic effects, our computational studies of the rheological response of the system have been limited to moderately confined geometries with $H > l$.

Our numerical simulations of the initially random ensemble of particles indicate that the distribution of particle periods is sharply peaked around the values corresponding to chains in the midplane of the channel. This form of the period distribution has important consequences for the rheological response of a suspension. In free space, the stress response of a dilute suspension of non-interacting axisymmetric particles to a sudden onset of steady shear flow is periodic, with a period that is the same as the period of particle trajectories. In contrast, the stress oscillations in a bounded suspension slowly

decay due to the phase shifts associated with the different lengths of the particle periods-such phase shifts randomize the initially coherent particle motion. Since the period distribution is sharply peaked, the decay of the oscillations of the stress response is slow, especially for weakly confined systems.

A dilute suspension of axisymmetric particles discussed here is a reference system for further investigations of the effect of Brownian motion, interparticle hydrodynamic interactions, and nonhydrodynamic forces on the dynamics of confined suspensions. We are studying the effects of binary particle collisions on the evolution of the particle distribution in a confined suspension under shear using a Boltzmann–Monte Carlo approach. Our preliminary results reveal an interesting behavior of the system, such as particle alignment with the vorticity direction, and the formation of layered particle ordering due to binary particle collisions. Similar ideas can also be applied to analyze suspensions undergoing Poiseuille flow in a parallel-wall channel.

ACKNOWLEDGMENTS

We would like to acknowledge the support of this work by NSF CAREER Grants CTS-0348175 (M.Z.G. and E.W.) and NASA Grant NAG-2704 (M.Z.G.).

References

Bhattacharya, S., J. Bławzdziewicz, and E. Wajnryb, "Hydrodynamic interactions of spherical particles in suspensions confined between two planar walls," J. Fluid Mech. **541**, 263–292 (2005a).

Bhattacharya, S., J. Bławzdziewicz, and E. Wajnryb, "Many-particle hydrodynamic interactions in parallel-wall geometry: Cartesian-representation method," Physica A **356**, 294–340 (2005b).

Bhattacharya, S., J. Bławzdziewicz, and E. Wajnryb, "Far-field approximation for hydrodynamic interactions in parallel-wall geometry," J. Comput. Phys. **212**, 718–738 (2006).

Bird, R., R. C. Armstrong, and O. Hassager, *Dynamics of Polymeric Liquids*, Vol. 1 (Wiley, New York, 1977).

Bławzdziewicz, J., and S. Bhattacharya, "Comment on Drift without flux: Brownian walker with a space-dependent diffusion coefficient," Europhys. Lett. **63**, 789–790 (2003).

Brenner, H., "Rheology of a dilute suspension of axisymmetric Brownian particles," Int. J. Multiphase Flow **1**, 195–341 (1974).

Bretherton, F., "The motion of rigid particles in a shear flow at low Reynolds number," J. Fluid Mech. **14**, 284–304 (1962).

Cichocki, B., and R. B. Jones, "Image representation of a spherical particle near a hard wall," Physica A **258**, 273–302 (1998).

Cichocki, B., R. B. Jones, R. Kutteh, and E. Wajnryb, "Friction and mobility for colloidal spheres in Stokes flow near a boundary: The multipole method and applications," J. Chem. Phys. **112**, 2548–2561 (2000).

Cohen, I., T. G. Mason, and D. A. Weitz, "Shear-induced configurations of confined colloidal suspensions," Phys. Rev. Lett. **93**, 046001 (2004).

Das, B., G. Enden, and G. Popel, "Stratified multiphase model for blood flow in a venular bifurcation," Ann. Biomed. Eng. **25**, 135–153 (1997).

Dufresne, E. R., D. Altman, and D. G. Grier, "Brownian dynamics of a sphere between parallel walls," Europhys. Lett. **53**, 264–270 (2001).

Durlofsky, L., J. F. Brady, and G. Bossis, "Dynamic simulation of hydrodynamically interacting particles," J. Fluid Mech. **180**, 21–49 (1987).

Einstein, A., "Eine Neue Bestimmung der Molikuldimensionen," Ann. Phys. **19**, 289–306 (1906).

Einstein, A., "Corrections," Ann. Phys. **34**, 591–592 (1911).

Frenkel, D., and B. Smit, *Understanding Molecular Simulation. From Algorithms to Simulations* (Academic, New York, 2002).

Gavze, E., and M. Shapiro, "Particles in shear flow near a solid wall: Effect of nonsphericity on forces and

velocities," Int. J. Multiphase Flow **23**, 155–182 (1997).
Gavze, E., and M. Shapiro, "Motion of inertial spheroidal particles in a shear flow near a solid wall with special application to aerosol transport in microgravity," J. Fluid Mech. **371**, 59–79 (1998).
Giddings, J., "Field–flow fractionation: Analysis of macromolecular, colloidal and particulate materials," Science **260**, 1456–1465 (1993).
Goldsmith, H., and S. Spain, "Margination of leukocytes in blood flow through small tubes," Microvasc. Res. **27**, 204–222 (1984).
Hernández-Ortiz, J., C. Stoltz, and M. Graham, "Transport and collective dynamics in suspensions of confined swimming particles," Phys. Rev. Lett. **95**, 204501 (2005).
Hsu, R., and P. Ganatos, "Gravitational and zero-drag motion of a spheroid adjacent to an inclined plane at low Reynolds number," J. Fluid Mech. **268**, 267–292 (1994).
Huang, L., E. Cox, R. Austin, and J. Sturm, "Continuous particle separation through deterministic lateral displacement," Science **304**, 987–990 (2004).
Jeffery, G., "The motion of ellipsoidal particles immersed in a viscous fluid," Proc. R. Soc. London, Ser. A **102**, 161–179 (1922).
Johnson, P. M., C. M. van Kats, and A. van Blaaderen, "Synthesis of colloidal silica dumbbells," Langmuir **21**, 11510–11517 (2005).
Kim, S., and S. J. Karrila, *Microhydrodynamics: Principles and Selected Applications* (Butterworth-Heinemann, London, 1991).
Kotaka, T., M. Kurata, and M. Tamura, "Normal stress effect in polymer solutions," J. Appl. Phys. **30**, 1705–1712 (1959).
Lançon, P., G. Batrouni, L. Lobry, and N. Ostrowsky, "Drift without flux: Brownian walker with a space-dependent diffusion coefficient," Europhys. Lett. **54**, 28–34 (2001).
Leal, L., and E. Hinch, "The effect of weak Brownian rotations on particles in shear flow," J. Fluid Mech. **46**, 685–703 (1971).
Lin, B., J. Yu, and S. A. Rice, "Direct measurements of constrained Brownian motion of an isolated sphere between two walls," Phys. Rev. E **62**, 3909–3919 (2000).
Loveland, J. P., S. Bhattacharjee, J. N. Ryan, and M. Elimelech, "Colloid transport in a geochemically heterogeneous porous medium: Aquifer tank experiment and modeling," J. Contam. Hydrol. **65**, 161–182 (2003).
Mody, N. A., and M. R. King, "Three-dimensional simulations of a platelet-shaped spheroid near a wall in shear flow," Phys. Fluids **17**, 113302 (2005).
Moses, K., S. Advani, and A. Reinhardt, "Investigation of fiber motion near solid boundaries in simple shear flow," Rheol. Acta **40**, 296–306 (2001).
Mucha, P. J., S. Y. Tee, D. A. Weitz, B. I. Shraiman, and M. P. Brenner, "A model for velocity fluctuations in sedimentation," J. Fluid Mech. **501**, 71–104 (2004).
Nguyen, N. Q., and A. J. C. Ladd, "Sedimentation of hard-sphere suspensions at low Reynolds number," J. Fluid Mech. **525**, 73–104 (2005).
Perktold, K., "On the paths of fluid particles in an axisymmetrical aneurysm," J. Biomech. **20**, 311–317 (1987).
Petrie, C., "The rheology of fibre suspensions," J. Non-Newtonian Fluid Mech. **87**, 369–402 (1999).
Pozrikidis, C., "Orbiting motion of a freely suspended spheroid near a plane wall," J. Fluid Mech. **541**, 105–114 (2005).
Press, W., S. Teukolsky, and W. Vetterling, *Numerical Recipes in C: The Art of Scientific Computing* (Cambridge University Press, New York, 1992).
Pries, A., K. Ley, M. Claassen, and P. Gaehtgens, "Red cell distribution at microvascular bifurcations," Microvasc. Res. **38**, 81–101 (1989).
Regazzetti, A., M. Hoyos, and M. Martin, "Influence of operating parameters on the retention of chromatographic particles by thermal field-flow fractionation," Anal. Chem. **76**, 5787–5798 (2004).
Staben, M. E., A. Z. Zinchenko, and R. H. Davis, "Dynamic simulation of spheroid motion between two parallel plane walls in low-Reynolds-number Poiseuille flow," J. Fluid Mech. **553**, 187–226 (2006).
Whitesides, G. M., and A. Stroock, "Flexible methods for microfluidics," Phys. Today **54**(6), 42–48 (2001).
Xia, Y. N., Y. D. Yin, Y. Lu, and J. McLellan, "Template-assisted self-assembly of spherical colloids into complex and controllable structures," Adv. Funct. Mater. **13**, 907–918 (2003).